

Domain decomposition improvement of quark propagator estimation

Tommy Burch, Christian Hagen

Institut für Theoretische Physik, Universität Regensburg, D-93040 Regensburg, Germany

Abstract

Applying domain decomposition to the lattice Dirac operator and the associated quark propagator, we arrive at expressions which, with the proper insertion of random sources therein, can provide improvement to the estimation of the propagator. Schemes are presented for both open and closed (or loop) propagators. In the end, our technique for improving open contributions is similar to the “maximal variance reduction” approach of Michael and Peisa, but contains the advantage, especially for improved actions, of dealing directly with the Dirac operator. Using these improved open propagators for the Chirally Improved operator, we present preliminary results for the static-light meson spectrum. The improvement of closed propagators is modest: on some configurations there are signs of significant noise reduction of disconnected correlators; on others, the improvement amounts to a smoothening of the same correlators.

Key words: Lattice gauge theory, hadron spectroscopy

1 Introduction

In recent years, there has been a number of techniques developed for improving estimates of quark propagators on the lattice (see, e.g., Refs. [1,2,3,4]). The main idea is to try to devise an estimator formulation which allows one to use all (or at least many) lattice sites as source locations for the quarks, rather than just having a fixed location, which is traditionally the case. If successful, one then has an estimate of the quark propagators from anywhere to anywhere in the lattice (typically called “all-to-all” propagators).

In the following sections we add our voices to the crowd and present our own method, which is based, foremostly, upon domain decomposition, or more specifically, the decomposition of block matrices. We end up with two different

types of estimators: one for “open” propagators between two domains of the lattice (or “half-to-half”) and one for “closed” propagators within one of the domains.

We first show how we devised our method through the consideration of random sources. Later we present first results for the two types of estimators and some of their possible applications: static-light mesons for the open propagators and disconnected correlators for the closed.

2 The method

Using a set of random sources, $\chi_{j\beta b}^n$, placed at all sites of the lattice, one can determine a corresponding set of solution vectors (we use a summation convention for repeated indices throughout this paper):

$$\eta_{i\alpha a}^n = M_{i\alpha a j\beta b}^{-1} \chi_{j\beta b}^n \quad (n = 1, \dots, N). \quad (1)$$

Since we know that $\lim_{N \rightarrow \infty} \frac{1}{N} \chi_{j\beta b}^n \chi_{k\gamma c}^{n\dagger} = \delta_{jk} \delta_{\beta\gamma} \delta_{bc}$, we can construct an estimate of the full propagator:

$$M_{i\alpha a k\gamma c}^{-1} \approx \frac{1}{N} \eta_{i\alpha a}^n \chi_{k\gamma c}^{n\dagger}. \quad (2)$$

This is, however, a rather noisy estimator and we map out some improvement schemes in the following sections.

The main feature of our approach involves the consideration of independent regions of the lattice, or domain decomposition, a technique used previously for “maximal variance reduction” (MVR) of pseudofermion estimators [1]. Similar considerations may also be used for improving dynamical lattice updates [5].

We can think of the lattice as a disjoint union of two regions. The full Dirac matrix can then be written in terms of submatrices

$$M = \begin{pmatrix} M_{11} & M_{12} \\ M_{21} & M_{22} \end{pmatrix}, \quad (3)$$

where M_{11} and M_{22} connect sites within a region and M_{12} and M_{21} connect sites from the different regions. (For simplicity, we suppress color, spin, and site indices in the following.) Regardless of the shape or nature¹ of the regions, a similarity transformation is all that is needed to reach this form. We can

¹ For example, different regions in color or Dirac space.

also write the propagator in this form:

$$M^{-1} = P = \begin{pmatrix} P_{11} & P_{12} \\ P_{21} & P_{22} \end{pmatrix}. \quad (4)$$

2.1 Open contributions

It is helpful to imagine reconstructing the sources in one region, χ_1^n , from the solution vectors everywhere, η^n , and to separate the contributions from the different regions:

$$\chi_1^n = M\eta^n = M_{11}\eta_1^n + M_{12}\eta_2^n. \quad (5)$$

If we now apply the inverse of the matrix within one region, we have

$$M_{11}^{-1}\chi_1^n = \eta_1^n + M_{11}^{-1}M_{12}\eta_2^n. \quad (6)$$

This can be solved for η_1^n and substituted into the original expression for the noisy estimator of the propagator between the two regions:

$$\begin{aligned} (M^{-1})_{12} &= P_{12} \approx \frac{1}{N}\eta_1^n\chi_2^{n\dagger} \\ &\approx \frac{1}{N} \left[M_{11}^{-1}(\chi_1^n - M_{12}\eta_2^n) \right] \chi_2^{n\dagger} \\ &\approx -\frac{1}{N} (M_{11}^{-1}M_{12}\eta_2^n) \chi_2^{n\dagger}, \end{aligned} \quad (7)$$

where in the last line we eliminate the first term due to the fact that we expect $\lim_{N \rightarrow \infty} \chi_1^n\chi_2^{n\dagger} = 0$. This is a crucial step, for here we cut out of the calculation what amounts to being only noise. It does not come for free, however, since we must perform the additional inversion within the subvolume 1. Writing out the full expression, we obtain

$$\begin{aligned} P_{12} &\approx -\frac{1}{N}M_{11}^{-1}M_{12}P\chi_2^n\chi_2^{n\dagger} \\ &= -M_{11}^{-1}M_{12}P_{22}, \end{aligned} \quad (8)$$

where the second line is an exact expression, showing that one can relate elements of different regions of $P = M^{-1}$ via the inverse of a submatrix of M . (We do not pretend to have derived something new here; after all, P_{22} is the Schur complement of M_{11}^{-1} . We only wish to emphasize the useful connection with random-source techniques.) Again, the lesson learned up to this point is that we need no sources in one of the two regions. The story does not end here, however.

Looking again at Eq. (8), one can see that we need not make the approximation $P_{22} \approx \frac{1}{N} P \chi_2^n \chi_2^{n\dagger}$. Instead, we can place the approximate Kronecker delta between the M_{12} and P_{22} :

$$\begin{aligned}
P_{12} &\approx -\frac{1}{N} M_{11}^{-1} M_{12} \chi_2^n \chi_2^{n\dagger} P \\
&\approx -\frac{1}{N} \left(M_{11}^{-1} M_{12} \chi_2^n \right) (\gamma_5 P \gamma_5 \chi_2^n)^\dagger \\
&\approx -\frac{1}{N} \psi_1^n \phi_2^{n\dagger}, \tag{9}
\end{aligned}$$

where we have used the γ_5 -hermiticity of the propagator (this is done only for convenience since we could just as well work with $P^\dagger \chi_2^n$ in the ϕ_2^n). From the next to last line, one can see that the signal only rises from terms where the two components of the χ_2^n 's are the same. However, unlike the naive estimator, Eq. (2), where there is only 1 such term giving a signal-to-noise of $\sim 1/V^{1/2}$, here there are many: for V_χ source points, the signal-to-noise is $\sim V_\chi / (V_\chi^2 - V_\chi)^{1/2} \sim 1$. Terms where the components of the sources are not the same can still be eliminated by ‘‘dilution’’ of the original source vectors, χ^n , that go into the ψ_1^n , the ϕ_2^n , or for greater noise reduction, both simultaneously. Probably more important than these considerations, however, is the fact that, for most of the propagators between the regions, the random sources are kept far from the end points. Also, one can use all points in one region for the source and all points in the other region for the sink.

The ideal domain decomposition for quark propagators which contribute to connected diagrams is then to use two unequal volumes, one containing a few more time slices (those of the sources χ) than the other. Ideally, the centers of the two sets of source time slices should be separated by $T/2$. The number of source time slices is dictated by the lattice Dirac operator since the χ 's should be placed on all time slices which communicate with the other region via one application of M . For Wilson and Fixed-Point (FP) [7] quarks, this is just 2 time slices, 1 adjacent to each boundary. For Chirally Improved (CI) quarks [6], which we use here, 4 are necessary (see Fig. 1). For the Asqtad action [8], 6 are needed due to the presence of the Naik term. While for Overlap fermions [9], it might be best to use equal volumes for the two regions since the sources will have to cover one region entirely. But we stress that for all of the above, one is free to dilute further: e.g., by inverting the sources on the different time slices separately.

For our first attempt of using this method, we do not choose the ideal decomposition. We use equal volumes for the two regions and place sources next to the boundaries in both regions (see Fig. 2). Although this choice may not be ideal, we do perform inversions for each spin component separately (spin dilution). Note also that, since our sources occupy all relevant time slices sur-

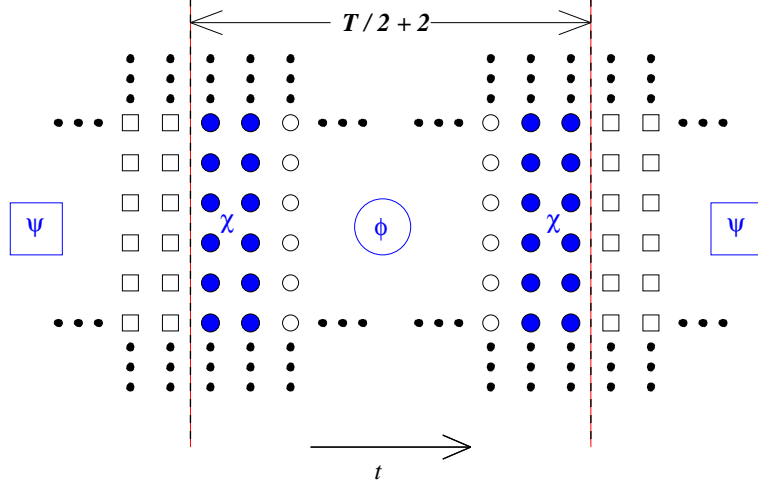


Fig. 1. Depiction of the ideal decomposition and the sources (χ) which are needed to construct the estimate of the CI quark propagator between regions.

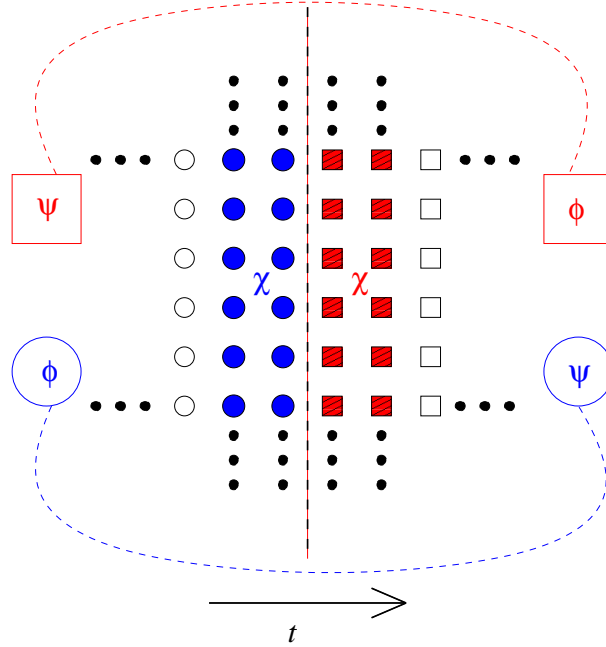


Fig. 2. Depiction of one of the boundaries and the surrounding sources (χ) which we use to construct the two estimates of the CI quark propagator between regions of equal volume. Colors and shapes indicate which source region contributes to the signal in the resultant vectors. The ψ 's are calculated using only one of the source regions, while the ϕ 's use both.

rounding the boundaries, we can actually obtain two independent estimates of the quark propagator between the two regions:

$$-\frac{1}{N}\psi_1^n\phi_2^{n\dagger} \approx P_{12} \approx -\frac{1}{N}\gamma_5\phi_1^n\psi_2^{n\dagger}\gamma_5. \quad (10)$$

So our method is very similar to that of MVR, except for the fact that we can work directly with M , instead of $M^\dagger M$. This gives the current method three advantages: First, it is less problematic to invert M since it has a better condition number than $M^\dagger M$ [1]. Second, implementing the method is straightforward. One needs only to limit the range of application of M when performing inversions in the subvolumes and when multiplying by the matrix between regions. Otherwise, existing routines remain unchanged. Third, the sources need only occupy enough time slices to connect them with the other region via M , rather than $M^\dagger M$. These are the same number of sources for Wilson-like operators, where $M^\dagger M$, like M , only extends one time slice. However, for many other improved operators (like CI and FP) this can reduce the number of necessary source time slices by a factor of 2.

2.2 Closed contributions

Working with the propagator within one of the regions, say 1, and following a similar derivation as in the previous section, one obtains an expression potentially useful for estimating quark propagators which return to the same region:

$$\begin{aligned} P_{11} &\approx \frac{1}{N} M_{11}^{-1} (\chi^n \chi_1^{n\dagger} - M_{12} P \chi^n \chi_1^{n\dagger}) \\ &= M_{11}^{-1} - M_{11}^{-1} M_{12} P_{21}. \end{aligned} \quad (11)$$

So once again, through the consideration of random sources, we arrive at an exact expression (and again, one which is nothing new). Now, combining the expressions for P_{11} and P_{21} ($= \gamma_5 P_{12}^\dagger \gamma_5$), we arrive at the relation:

$$P_{11} = M_{11}^{-1} + M_{11}^{-1} M_{12} \gamma_5 (M_{11}^{-1} M_{12} P_{22})^\dagger \gamma_5. \quad (12)$$

Inserting our random sources into this expression gives

$$\begin{aligned} P_{11} &\approx M_{11}^{-1} + \frac{1}{N} (M_{11}^{-1} M_{12} \gamma_5 \chi_2^n) (\gamma_5 M_{11}^{-1} M_{12} P \chi^n)^\dagger \\ &\approx M_{11}^{-1} + \frac{1}{N} \zeta_1^n \theta_1^{n\dagger}. \end{aligned} \quad (13)$$

Note that we put no region index on the second χ , indicating that for this resultant vector (θ_1) we wish to use sources initially placed everywhere on the lattice. The advantage of expression (13) may not be immediately clear since it still contains the explicit appearance of M_{11}^{-1} .

This seeming hindrance can be remedied by considering a very small volume for region 1. Performing this ‘‘highly reduced’’ inversion exactly, we hope to

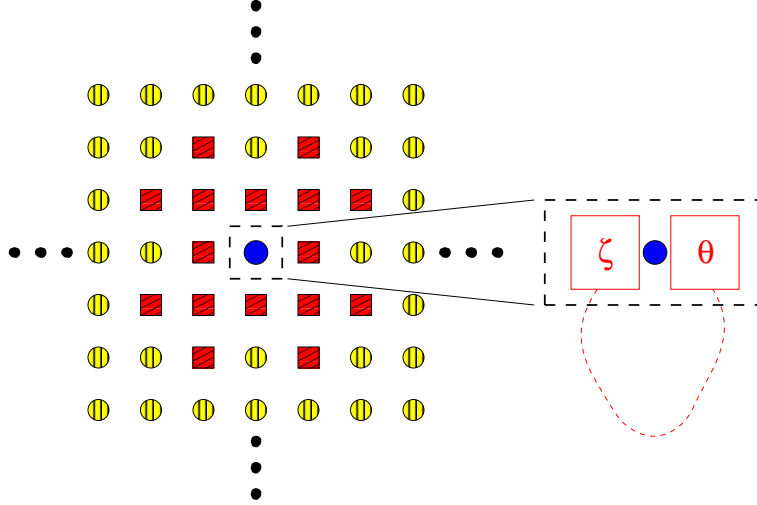


Fig. 3. Depiction of the boundary and the surrounding region of sources which are needed to construct the estimated CI quark propagator to and from the central point. In this figure, region 1 is just one site (we also consider a larger region which includes nearest neighbors). The red squares indicate which region of sources contributes to the signal in the resultant vectors (ζ_1, θ_1) of Eq. (13).

find a significant gain in the signal-to-noise ratio: The first term in the above expressions will be exact and the second term, as compared to its naive estimate, may be improved by a factor of as much as $\sim V_\chi^{1/2}$, where V_χ is now the volume of sources in region 2 which connect to region 1 via M . So if the volume of region 1 is kept small enough and the lattice Dirac operator connects each site to many others, there may be an advantage to calculating the M_{11}^{-1} 's exactly, as opposed to simply inverting more sources.

Here, we propose to use spin-diluted, but full-volume sources for χ , so that we can, in the end, use all sites as the starting and ending point of the propagator P_{xx} with only N original full-volume inversions: the $P\chi^n$ in θ_1^n . We can consider the smallest, symmetrical volume for region 1, the point itself ($V_1 = 1$; see Fig. 3), in order to reduce the amount of work needed to calculate M_{11}^{-1} , which we need for each point in the lattice. With this choice, at most one needs to invert V 12×12 matrices. Since $V_\chi = 128$ for the CI operator in this scenario, we hope that this small amount of extra work may be worth the effort. In the end, however, we actually use a larger region 1, including nearest neighbors ($V_1 = 9$), but we avoid some extraneous work by only inverting M_{11} upon 12 sources located at the central point.

3 First results

In this section, we present some first results obtained with our estimated quark propagators. We first use the open propagators for the light quark in heavy-

Table 1

Static-light meson operators.

oper.	J^P	$\bar{Q} O(\Gamma, D_i) q'$
S	$0^-, 1^-$	$\bar{Q} \gamma_5 q'$
P_-	$0^+, 1^+$	$\bar{Q} \sum_i \gamma_i D_i q'$
P_+	$1^+, 2^+$	$\bar{Q} (\gamma_1 D_1 - \gamma_2 D_2) q'$
D_\pm	$1^-, 2^-, 3^-$	$\bar{Q} \gamma_5 (D_1^2 - D_2^2) q'$

light meson correlators, where we use the static approximation for the heavy quark. We also show the effects of using our closed propagators in disconnected correlators.

3.1 Static-light mesons

For our meson source and sink operators, we use bilinears of the form:

$$\bar{Q} O(\Gamma, D_i, \vec{D}^2, S) q, \quad (14)$$

where S is a gauge-covariant (Jacobi) smearing operator [10] and \vec{D} is the covariant derivative. For our basis of light-quark spatial wavefunctions, we use three different amounts of smearing and apply 0, 1, and 2 covariant Laplacians to these:

$$q' = S_8 q, \quad \vec{D}^2 S_{12} q, \quad \vec{D}^2 \vec{D}^2 S_{16} q, \quad (15)$$

where the subscript on the smearing operator denotes the number of smearing steps; all are applied with the same weighting factor of $\kappa_{sm} = 0.2$. So we have a relatively narrow, approximately Gaussian distribution, along with wider versions which exhibit one and two radial nodes, due to the application of the Laplacians. We point out that, thus far, we have not altered the quantum numbers of the meson source since both the smearing and Laplacians treat all spatial directions the same (i.e., they are scalar operations). In order to create mesons of different quantum numbers, we use these light-quark distributions together with the operators shown in Table 1 (see, e.g., Ref. [1]).

Inserting the estimated and static propagators in the meson correlators we have

$$\begin{aligned} C_{ij}(t) &= \langle 0 | (\bar{Q} O_j q)_t (\bar{q} \bar{O}_i Q)_0 | 0 \rangle \\ &= \left\langle \sum_x \text{Tr} \left[\frac{1 + \gamma_4}{2} \prod_{i=0}^{t-1} U_4^\dagger(x + i\hat{4}) O_j P_{x+t\hat{4}, x} \bar{O}_i \right] \right\rangle_{\{U\}}. \end{aligned} \quad (16)$$

The static quark is propagated through products of links in the time direction

and has a fixed spin $(1 + \gamma_4)/2$. The estimated propagator $P_{x+t\hat{4},x}$ is of the form of Eq. (10). Thus, all points within region 1 ($N_s^3 N_t/2$ of them) can act as the source location x , just so long as t is large enough to have the sink location $x + t\hat{4}$ in region 2. Note that we now have subscripts on the source and sink operators to denote which light-quark distribution is being used. We create all such combinations and thus have a 3×3 matrix of correlators for each of the operators in Table 1.

Following the work of Michael [11] and Lüscher and Wolff [12], we use this cross-correlator matrix in a variational approach to separate the different mass eigenstates. We must therefore solve the generalized eigenvalue problem

$$C(t)\vec{v}^{(k)} = \lambda^{(k)}(t, t_0) C(t_0)\vec{v}^{(k)}, \quad (17)$$

in order to obtain the following eigenvalues:

$$\lambda^{(k)}(t, t_0) \propto e^{-tM_k} [1 + O(e^{-t\Delta M_k})], \quad (18)$$

where M_k is the mass of the k th state and ΔM_k is the mass-difference to the next state. For large enough values of t , each eigenvalue should then correspond to a unique mass state, requiring only a single-exponential fit.

Before solving the above eigenvalue problem, we check that our cross-correlator matrix is real and symmetric (within errors). We then make it symmetric before solving Eq. (17) and look for regions of t where the eigenvalues exhibit single masses and the corresponding eigenvectors, $\vec{v}^{(k)}$, are stable (each of these provides what we call the “fingerprint” of a state and if it holds steady, we have better reason to believe that we are looking at a single state). The results should be independent of the normalization time slice t_0 and we make sure that this is so. For our final results, however, we use the value of $t_0/a = 1$.

This variational approach has seen much use recently in lattice QCD, especially for extracting excited hadron masses and we point the reader to the relevant literature in [13].

We create our cross-correlator matrices on two sets of gluonic configurations: 100 quenched and 74 dynamical, each with $12^3 \times 24$ lattices sites. The quenched configurations have a lattice spacing of $a \approx 0.15$ fm ($a^{-1} \approx 1330$ MeV) and a spatial extent of $L \approx 1.8$ fm. The dynamical set [14] has 2 flavors of CI sea quarks (with $M_{\pi,\text{sea}} \approx 500$ MeV), $a \approx 0.115$ fm ($a^{-1} \approx 1710$ MeV), and $L \approx 1.4$ fm. We use 12 random spin-color vectors as sources for the light-quark propagator estimation. Spin-diluted, this gives us 48 separate sources for the inversions (one in the full volume, ϕ , and two in the subregions, ψ ; see Eqs. (9) and (10)). We perform inversions for 4 different quark masses: $am_q = 0.02, 0.04, 0.08, 0.10$.

After extracting the eigenvalues, we check for single mass states by creating

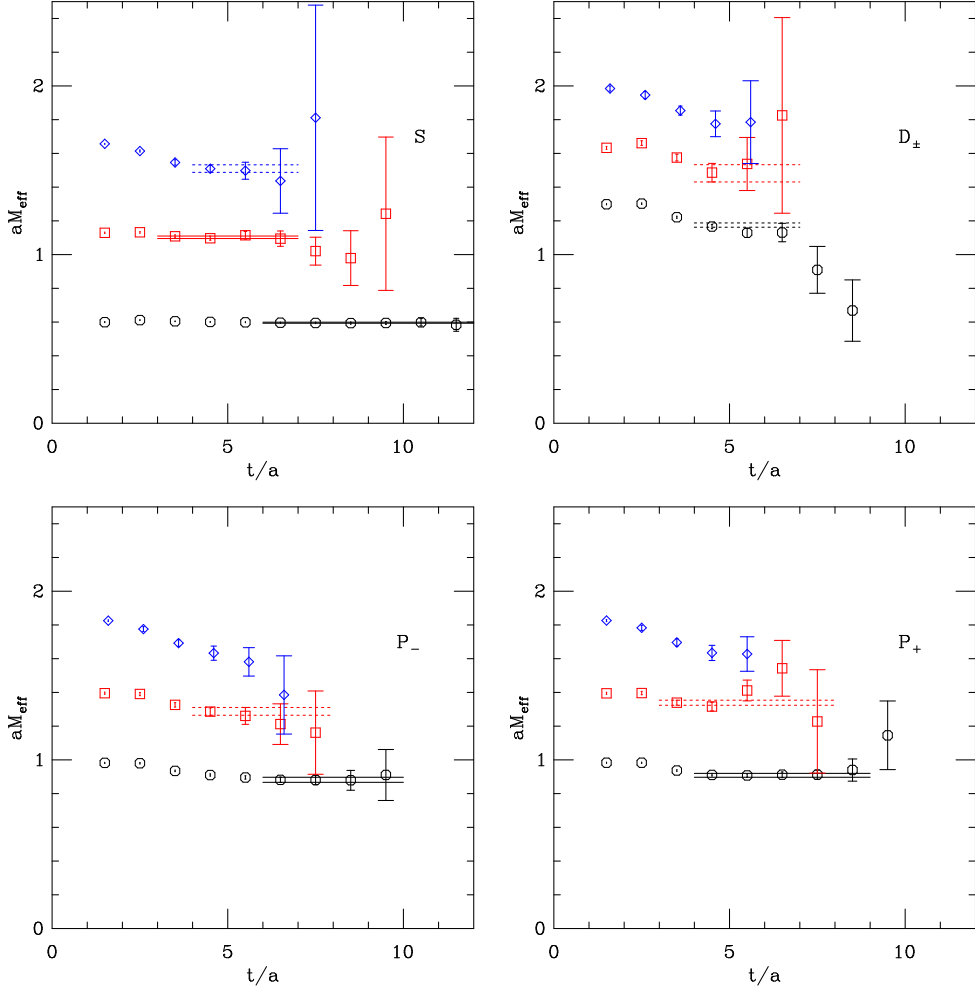


Fig. 4. Effective masses for the static-light mesons on the quenched configurations. $am_q = 0.08$, $a^{-1} \approx 1330$ MeV, $L \approx 1.8$ fm. The horizontal lines represent $M \pm \sigma_M$ fit values for the corresponding time ranges. Dashed lines indicate fits for which we adjust the minimum time for systematic error estimates.

effective masses:

$$aM_{\text{eff}}^{(k)}\left(t + \frac{1}{2}\right) = \ln\left(\frac{\lambda^{(k)}(t)}{\lambda^{(k)}(t+1)}\right). \quad (19)$$

A representative sample of these, along with single-elimination jackknife errors, are plotted against time in Figures 4 and 5. In each case one finds values from the first two or three eigenvalues. The horizontal lines signify the $M \pm \sigma_M$ values which result from correlated fits over the corresponding range in time (dashed lines denote fits where we also later increased the minimum time of the fit in order to estimate systematic errors). We require that at least three effective mass points display a plateau (within errors) and that the eigenvectors remain constant over the same range before we perform said fits. Figure 6 shows the eigenvector components for the quenched first-excited P -wave

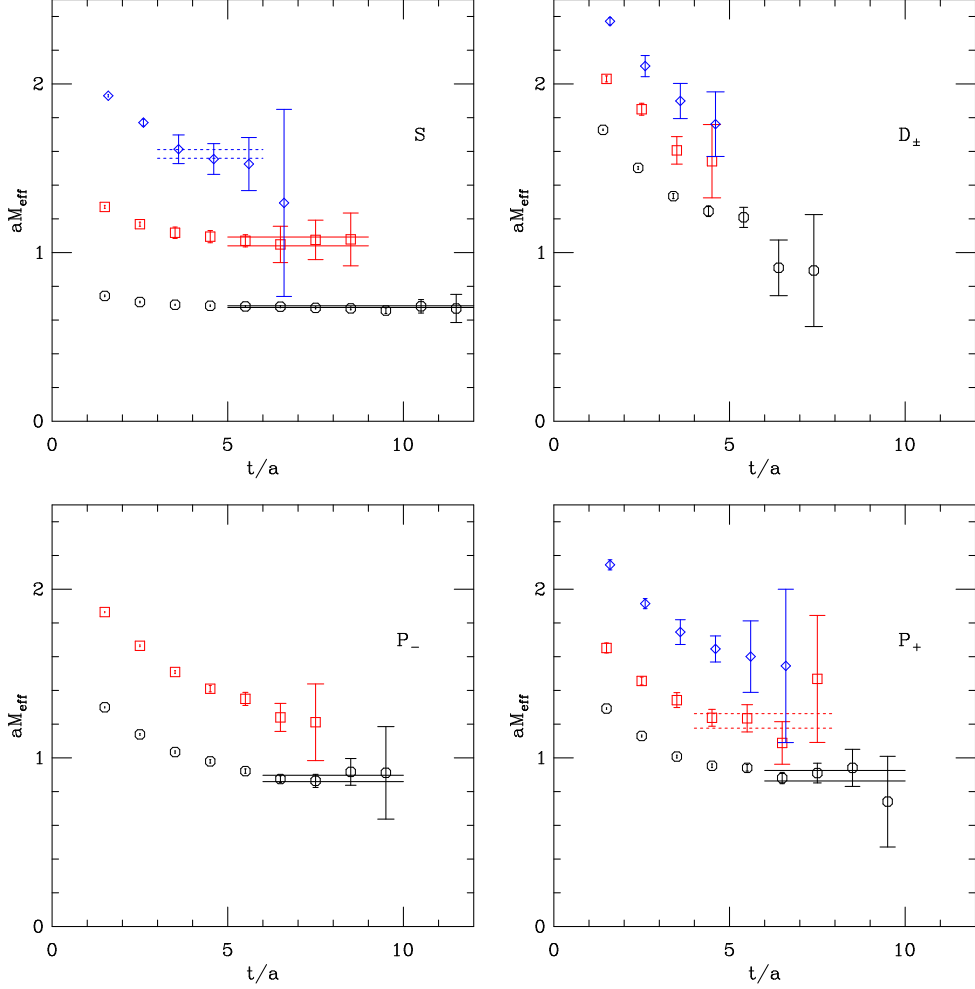


Fig. 5. Effective masses for the static-light mesons on the dynamical ($M_{\pi,\text{sea}} \approx 500$ MeV) configurations. $am_q = 0.08$, $a^{-1} \approx 1710$ MeV, $L \approx 1.4$ fm. The horizontal lines represent $M \pm \sigma_M$ fit values for the corresponding time ranges. Dashed lines indicate fits for which we adjust the minimum time for systematic error estimates.

($2P_+$), a state displaying a rather jumpy effective-mass plateau. There is some slight variation in the central values over time, but when considering the fine scale of the plots and the errors, we are confident that we are dealing with a single state.

Performing fits for all quark masses, we next take a look at the mass splittings ($M - M_{1S}$) as a function of the quark mass. These are plotted in Figure 7, along with the chirally extrapolated results ($m_q \rightarrow 0$). We use simple linear fits to perform these extrapolations (as well as for the interpolations to $m_q = m_s$) since there appears to be little scaling in these plots. Both sets of results display a clear ordering of alternating parities with increasing mass. The quenched $2S$ and $1D_{\pm}$ states are close, with the latter being slightly higher in mass. This is expected since the D_{\pm} represents an average of higher spins than the S and the heavy-quark spin interactions which would “mix” the purely orbitally excited

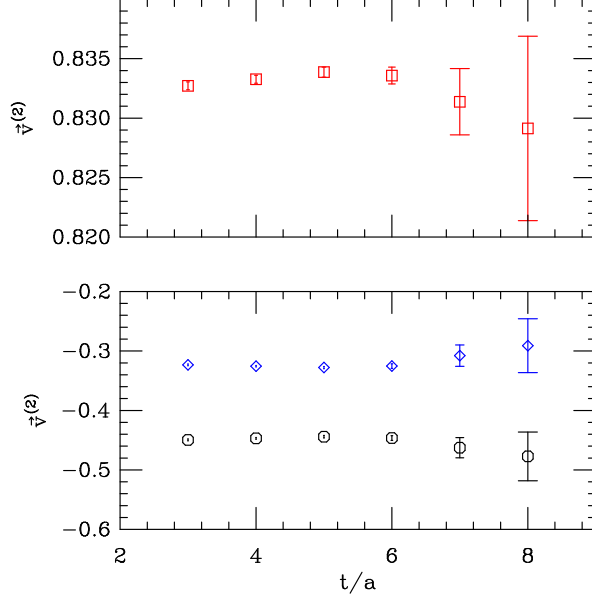


Fig. 6. The three eigenvector components for the quenched $2P_+$ state over the time range of the fit.

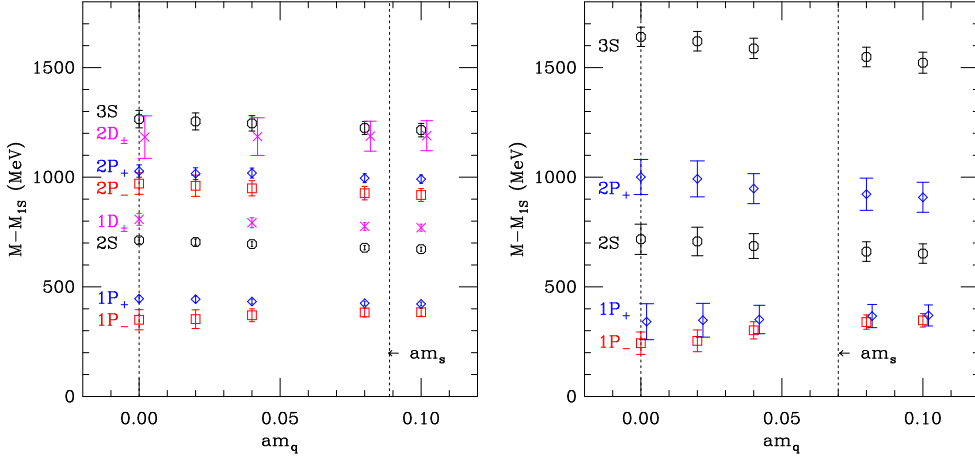


Fig. 7. Physical mass splittings ($M - M_{1S}$) as a function of the quark mass for the quenched (left) and dynamical (right) lattices. The vertical lines denote the chiral limit ($m_q \rightarrow 0$) and the strange quark mass (m_s). The left-most values are the (linear) chiral extrapolations. All errors are only statistical for the chosen fit ranges.

D -waves with the ground-state S -wave are absent in the static approximation. Overall, the results for the dynamical configurations are poorer. This is no big surprise since here we have not only fewer configurations, but also a smaller physical volume ($L \approx 1.4$ fm). This fact also makes it difficult, at least at the present stage, to discern quenching and finite-volume effects. However, the one marked difference, the jump in the $3S$ mass, is quite likely due to the smaller volume.

Table 2

Mass splittings for our B mesons ($m_q \rightarrow 0$). The first number in parentheses is the statistical error. The second set (if present) are the additional systematic errors which result from adjustments to the minimum time of the fit.

state	J^P	$M - M_{1S}$ (MeV)		
		$N_f = 0, L \approx 1.8$ fm	$N_f = 2, L \approx 1.4$ fm	PDG [15]
$2S$	$0^-, 1^-$	712(14)	717(69)	-
$3S$	$0^-, 1^-$	1265(40)($^{+0}_{-130}$)	1640(44)($^{+55}_{-200}$)	-
$1P_-$	$0^+, 1^+$	350(46)	243(51)	384(8)
$2P_-$	$0^+, 1^+$	971(49)($^{+50}_{-90}$)	-	-
$1P_+$	$1^+, 2^+$	446(15)	341(82)	384(8)
$2P_+$	$1^+, 2^+$	1028(28)($^{+160}_{-80}$)	1001(80)($^{+130}_{-20}$)	-
$1D_\pm$	$1^-, 2^-, 3^-$	808(27)($^{+0}_{-90}$)	-	-
$2D_\pm$	$1^-, 2^-, 3^-$	1183(97)($^{+130}_{-150}$)	-	-

In Tables 2 and 3 we present the results for the chirally extrapolated (B mesons) and strange-quark-mass interpolated (B_s mesons) mass splittings. We include the statistical errors from the fits in the first set of parentheses. For fits where the effective-mass plateaus are not immediately clear (e.g., fits represented with dashed lines in Figures 4 and 5), we move the minimum time of the fit range out by one to two time slices and observe the subsequent changes in $M \pm \sigma_M$, as compared to the previous values. The differences from the old values are reported as systematic errors; these appear in the second set of parentheses.

It is interesting to note that, in moving from the quenched lattices to the smaller, dynamical lattices, the $M_{2S} - M_{1S}$ mass splitting remains unchanged. Unless there is an odd counter-balancing of finite-volume and quenching effects between the lattices, we may conclude that our values for $M_{2S} - M_{1S}$ are reliable. The same is true for the $M_{2P} - M_{1S}$ splitting, which is a bit strange since $M_{1P} - M_{1S}$ already shows a difference, its value becoming especially low for the $1P_-$, when compared with the result from experiment (the quantum numbers, J^P , for the experimentally observed, excited B and B_s mesons have yet to be confirmed, so we place them in both the $1P_-$ and $1P_+$ rows). For our B_s mesons, all $M_{1P} - M_{1S}$ splittings appear to be too small. Better statistics and larger volumes are needed if we are to clearly resolve these matters.

One thing is clear though: due to the improvement of the light-quark propagator estimation, and our subsequent ability to use half the points of the lattice as source locations, we have greatly improved our chances of isolating excited heavy-light states. In an earlier study [16] of heavy-light mesons using wall sources on the same quenched configurations, we were barely able to see the

Table 3

Mass splittings for our B_s mesons ($m_q = m_s$). The first number in parentheses is the statistical error. The second set (if present) are the additional systematic errors which result from adjustments to the minimum time of the fit.

state	J^P	$M - M_{1S}$ (MeV)		
		$N_f = 0, L \approx 1.8$ fm	$N_f = 2, L \approx 1.4$ fm	PDG [15]
$2S$	$0^-, 1^-$	675(10)	665(45)	-
$3S$	$0^-, 1^-$	1220(30)($^{+20}_{-50}$)	1560(45)($^{+35}_{-190}$)	-
$1P_-$	$0^+, 1^+$	384(20)	330(34)	448(16)
$2P_-$	$0^+, 1^+$	923(30)($^{+10}_{-60}$)	-	-
$1P_+$	$1^+, 2^+$	424(10)	363(55)	448(16)
$2P_+$	$1^+, 2^+$	993(20)($^{+130}_{-50}$)	930(75)($^{+0}_{-80}$)	-
$1D_\pm$	$1^-, 2^-, 3^-$	773(17)($^{+0}_{-80}$)	-	-
$2D_\pm$	$1^-, 2^-, 3^-$	1188(68)($^{+170}_{-80}$)	-	-

$2S$ state, let alone the excited states in any other operator channel. Also, there we used NRQCD for the heavy quark; this should only boost the signals since the heavy quark can then “explore” more of the lattice through its kinetic term. It is obvious, however, that we have much better signals now since we are able to see excited states in every channel ($2S$, $3S$, $2P_-$, $2P_+$, and $2D_\pm$) on the quenched lattice.

3.2 Disconnected correlators

As a preliminary testing ground for our closed propagators, we take a look at some first results for the disconnected contributions to pseudoscalar ($J^P = 0^-$) meson correlators:

$$D(t) = \sum_{t_0, \vec{x}, \vec{y}} \text{Tr}(\gamma_5 P_{\vec{x}, t_0; \vec{x}, t_0}) \text{Tr}(\gamma_5 P_{\vec{y}, t_0+t; \vec{y}, t_0+t}). \quad (20)$$

Again, we use 12 random spin-color sources (initially placed everywhere on the lattice), spin-dilute them, and perform inversions ($P\chi^n$) at a quark mass of $am_q = 0.02$ on the quenched configurations. We then condition these “naive” estimates via Eq. (13) using the central point and its nearest neighbors (NN) as region 1 (the calculation of all the M_{11}^{-1} ’s for this sized region on a single configuration takes less than a day on a PC).

In Figure 8 we compare results obtained via the naive and improved estimators on two different quenched configurations. The errors are estimated via the

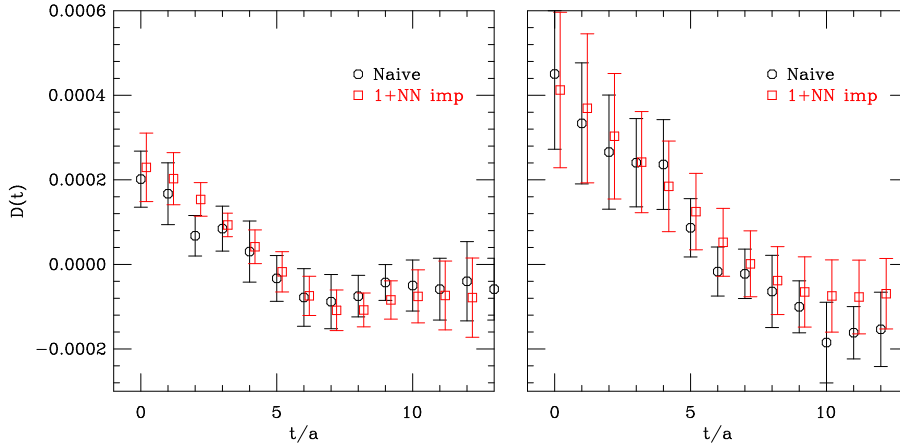


Fig. 8. Naive and improved disconnected pseudoscalar correlators (with $am_q = 0.02$) on two different quenched configurations. Errors result from a single-elimination jackknife procedure over the 12 random spin-color sources.

single-elimination jackknife subsets of the 12 random sources. Looking at the result for the configuration on the left, we can see significant reduction of the errors over many time separations. This is not the case for all configurations, however, as one can see on the right, where the errors are comparable, if not slightly larger for the improved version. For both cases shown here (and in fact for all configurations) the central values for the improved method follow a smoother curve. This should be no great surprise since the improved estimator uses sources on neighboring time slices (see Figure 3), whereas the naive one does not. So the improved version should smoothen out some of the remaining fluctuations over different t values.

An important thing to note here is that, despite any of the improvement which we may gain from the smaller errors on some configurations and the smoothening of the curves, the error for the ensemble average of $D(t)$ will be dominated by the limited number of gauge configurations (i.e., this is a “gauge-limited” quantity). One can see from the figure that the fluctuation which comes from switching configurations is as big as, or bigger than, the jackknife errors from the sources. For some other configurations, the jump in the corresponding $D(t)$ values is much larger. These are perhaps configurations with large values of topological charge, Q ; after all, the integrated disconnected pseudoscalar correlator is related to the square of this quantity [17]:

$$\sum_t D(t) \propto \frac{Q^2}{m_q^2}, \quad (21)$$

where the relation is only approximate here since we use only chirally improved quarks.

Although we see no great overall improvement for these light, disconnected pseudoscalars, this is a tough testing ground. It remains to be seen how well

these improved closed propagators will perform for other quantities where only averages of single loops over single time slices are needed: e.g., $s\bar{s}$ loops within hadron correlators to measure strangeness content, an application which we plan to look into in the near future. We also point the interested reader to other improvement schemes for closed contributions: see, e.g., [18,19].

4 Summary

We have presented a method for improving the estimation of quark propagators in lattice QCD. The improvement we obtain for open propagators between equal subvolumes of the lattice is significant. The boost in statistics from being able to use up to half of the lattice sites as starting locations for our static-light meson correlators allows us to extract a number of radially and orbitally excited states ($2S$, $3S$, $1P$, $2P$, $1D$, $2D$).

As we have pointed out, our method is similar to the maximal variance reduction approach [1]. However, since we can work with the Dirac matrix M , rather than $M^\dagger M$, our method may be better suited for highly improved actions.

Although the first results for our improved closed propagators are not very promising, it appears that we have chosen a very difficult application (light, disconnected, pseudoscalar correlators) for which to test them. We reserve final judgment on their usefulness for the future, when we measure their performance in other physical quantities.

Acknowledgements

We would like to thank Christof Gatttringer for many helpful discussions. We are also indebted to our colleagues in Graz – Christian B. Lang, Wolfgang Ortner, and Pushan Majumdar – for sharing their dynamical CI configurations with us. We also wish to thank Andreas Schäfer for fostering a large research group, thereby making collaborations such as this possible. Simulations were performed on the Hitachi SR8000 at the LRZ in Munich. This work is supported by GSI.

5 Appendix A

In Section 2, we derived the exact relations (8) and (11) for the blocks of the quark propagator. In those derivations we relied upon the following property

of the random vectors χ_i^n , $n = 1, \dots, N$:

$$\lim_{N \rightarrow \infty} \left(\frac{1}{N} \chi_i^n \chi_j^{n\dagger} \right) = \delta_{ij}. \quad (22)$$

But there also exist other possibilities to derive the same results.

As an alternative, we show here how one can arrive at Eq. (8) using the path integral over the fermionic degrees of freedom.

The Dirac propagator, $P = M^{-1}$, can be represented by a path integral in the following way

$$P_{ij} = \frac{1}{Z} \int [D\psi][D\bar{\psi}] \psi_i \bar{\psi}_j e^{-S_f}, \quad (23)$$

where

$$Z = \int [D\psi][D\bar{\psi}] e^{-S_f}, \quad (24)$$

is the partition function, S_f is the fermion action

$$S_f = \bar{\psi} M \psi, \quad (25)$$

and $[D\psi] = \prod_k d\psi_k$ is the integration measure.

The first step in our alternative approach is to split the fermion action into a sum of four separate contributions:

$$S_f = \bar{\psi}_1 M_{11} \psi_1 + \bar{\psi}_2 M_{22} \psi_2 + \bar{\psi}_1 M_{12} \psi_2 + \bar{\psi}_2 M_{21} \psi_1. \quad (26)$$

The leading two contributions are only connecting the fermion fields within the regions 1 (R_1) and 2 (R_2), while the other two contributions provide the connections between the regions. In a similar way, one can also divide the integration measures in Eqs. (23) and (24).

When one now considers the special case of Eq. (23) when $i \in R_1$ and $j \in R_2$ and uses expression (26) the propagator becomes

$$\begin{aligned}
P_{12} &= \frac{1}{Z} \int [D\psi][D\bar{\psi}] \psi_1 \bar{\psi}_2 e^{-S_f} \\
&= -\frac{1}{Z} \int [D\psi_2][D\bar{\psi}_2] \bar{\psi}_2 e^{-\bar{\psi}_2 M_{22} \psi_2} \times \\
&\quad \int [D\psi_1][D\bar{\psi}_1] \psi_1 e^{-\bar{\psi}_1 M_{11} \psi_1 - \bar{\psi}_1 M_{12} \psi_2 - \bar{\psi}_2 M_{21} \psi_1} \\
&= -\frac{\det(M_{11})}{Z} \int [D\psi_2][D\bar{\psi}_2] \bar{\psi}_2 (-M_{11}^{-1} M_{12} \psi_2) e^{-\bar{\psi}_2 \tilde{M}_{22} \psi_2} \\
&= -\frac{\det(M_{11}) \det(\tilde{M}_{22})}{Z} M_{11}^{-1} M_{12} \tilde{M}_{22}^{-1}, \tag{27}
\end{aligned}$$

where M_{11} and $\tilde{M}_{22} := M_{22} - M_{21} M_{11}^{-1} M_{12}$ are the diagonal blocks of a decomposed version of M with 0's as off-diagonal blocks. Therefore, $Z = \det(M) = \det(M_{11}) \det(\tilde{M}_{22})$ and the ratio becomes 1. For the next to last step, we completed the square in the exponent and performed a shift of the integration measure.

Since \tilde{M}_{22} is the Schur complement of M_{11} , one can show that in fact $P_{22} = \tilde{M}_{22}^{-1}$. This leads us to our final result

$$P_{12} = -M_{11}^{-1} M_{12} P_{22}. \tag{28}$$

References

- [1] C. Michael and J. Peisa [UKQCD Collaboration], Phys. Rev. D 58 (1998) 034506.
- [2] A. Duncan and E. Eichten, Phys. Rev. D 65 (2002) 114502.
- [3] G. S. Bali, *et al.*, [SESAM Collaboration], Phys. Rev. D 71 (2005) 114513.
- [4] J. Foley, *et al.*, Comput. Phys. Comm. 172 (2005) 145.
- [5] M. Lüscher, Comput. Phys. Comm. 165 (2005) 199.
- [6] P. H. Ginsparg and K. G. Wilson, Phys. Rev. D 25 (1982) 2649; C. Gattringer, Phys. Rev. D 63 (2001) 114501; C. Gattringer, I. Hip, and C. B. Lang, Nucl. Phys. B 597 (2001) 451.
- [7] P. Hasenfratz, *et al.*, Int. J. Mod. Phys. C 12 (2001) 691; T. Jorg, Thesis, Bern University, 2002 [hep-lat/0206025].
- [8] K. Orginos, D. Toussaint, and R. L. Sugar [MILC Collaboration], Phys. Rev. D 60 (1999) 054503; G. P. Lepage, Phys. Rev. D 59 (1999) 074502.
- [9] H. Neuberger, Phys. Lett. B 417 (1998) 141; Phys. Rev. Lett. 81 (1998) 4060.

- [10] S. Güsken, *et al.*, Phys. Lett. B 227 (1989) 266; C. Best, *et al.*, Phys. Rev. D 56 (1997) 2743.
- [11] C. Michael, Nucl. Phys. B 259 (1985) 58.
- [12] M. Lüscher and U. Wolff, Nucl. Phys. B 339 (1990) 222.
- [13] S. Sasaki, T. Blum, and S. Ohta, Phys. Rev. D 65 (2002) 074503; D. Brömmel, *et al.*, Phys. Rev. D 69 (2004) 094513; T. Burch, *et al.* [BGR Collaboration], Phys. Rev. D 70 (2004) 054502; Phys. Rev. D 73 (2006) 017502; Phys. Rev. D 73 (2006) 094505; Phys. Rev. D 74 (2006) 014504; K. J. Juge, *et al.*, hep-lat/0601029.
- [14] C. B. Lang, P. Majumdar, and W. Ortner, Phys. Rev. D 73 (2006) 034507.
- [15] W.-M. Yao, *et al.*, J. Phys. G 33 (2006) 1.
- [16] T. Burch, C. Gattringer, and A. Schäfer, Nucl. Phys. Proc. Suppl. 140 (2005) 347.
- [17] R. G. Edwards, U. M. Heller, and R. Narayanan, Phys. Rev. D 59 (1999) 094510.
- [18] C. McNeile and C. Michael [UKQCD Collaboration], Phys. Rev. D 63 (2001) 114503.
- [19] T. A. DeGrand and U. M. Heller [MILC collaboration], Phys. Rev. D 65 (2002) 114501.